RESEARCH ARTICLE | SEPTEMBER 03 2020

Engineering the optical reflectance of randomly arranged self-assembled semiconductor nanowires

Valeria Demontis; Andrea Marini; Francesco Floris; Lucia Sorba; Francesco Rossella

AIP Conference Proceedings 2257, 020009 (2020)
https://doi.org/10.1063/5.0023675

Engineering the Optical Reflectance of Randomly Arranged Self-Assembled Semiconductor Nanowires

Valeria Demontis[1], Andrea Marini[2], Francesco Floris[3, a)], Lucia Sorba[1] and Francesco Rossella[1, b)]

[1] *NEST, Scuola Normale Superiore and Istituto Nanoscienze-CNR, Pisa, Italy.*
[2] *Department of Physical and Chemical Sciences, University of L'Aquila, L'Aquila, Italy.*
[3] *Tyndall National Institute - University College Cork, Cork, Ireland.*

[a)] Corresponding author: francesco.floris@tyndall.ie
[b)] Corresponding author: francesco.rossella@sns.it

Abstract. Metasurfaces made of arrays of vertically aligned semiconductor nanowires are suitable platforms for light management in optical and photonic applications. Here we report a design approach aimed at engineering the optical behavior of semiconductor nanowire ensembles randomly displaced on the substrate, in order to enhance modulation effects in their optical reflectance response. By resorting to analytical and numerical simulations we demonstrate that the combined implementation of a multi-shell layering together with a tapered designing on the individual nanowire offer new opportunities to tailor the optical reflectance oscillations in this kind of architectures. The simulation insights were compared to experimental results reported for self-assembled GaAs nanowires and GaAs/AlGaAs core-shell nanowires. The proposed approach is especially promising for epitaxially grown semiconductor nanowires, where the suggested design modifications can be easily implemented during the nanostructure growth.

INTRODUCTION

Metasurfaces made of arrays of sub-wavelength nanostructures or thin films have attracted great interest in recent years as they offer an unprecedented potential for the engineering of electromagnetic wave propagation, going well beyond the capabilities of natural materials [1-6]. Several approaches for designing metasurfaces have been reported, based on the use of metals, dielectric materials or composites [1,3,7,8]. Here we focus in particular on dielectric materials, which are often preferable as they have the advantage of lower optical losses [9-11]. Several promising applications have already been reported, such as reflectors [12], meta-lenses [13], nano-photonic devices [14], to name a few. In this context, systems based on ensembles of periodically aligned cylinder-shaped subwavelength nanostructures, such as porous semiconductors with a preferential pore alignment direction [15], nanotubes and nano-rods [16,17] and semiconductor nanowires (NWs) [18-20], have been proposed as promising material platforms for the modulation of the optical behavior in the far field, thanks to the collective optical response of individual scatterers. These systems have been applied to sensing [21], to light trapping enhancement in solar cells [22-24], to the control of light polarization [25], to the fabrication of dispersive holograms [26].

In this work, we focused on randomly arranged semiconductor NW arrays in order to propose a novel approach to the optical engineering of ensembles of vertically aligned nanostructures with cylindrical symmetry. Our goal is to introduce controlled modulations in the specular reflectance of these systems by opportune geometrical modifications in the individual building block shape. The efficacy of the proposed strategy and the physical phenomena occurring in the system were evaluated by means of simulation techniques, by using both an analytical approach, based on the Maxwell-Garnett effective medium theory, and by solving the Maxwell equation in the photonic systems by means of finite-difference time-domain (FDFT) numerical simulations. The starting point is a

NANOINNOVATION 2019
AIP Conf. Proc. 2257, 020009-1–020009-10; https://doi.org/10.1063/5.0023675
Published by AIP Publishing. 978-0-7354-2017-5/$30.00

basic configuration made of a random ensemble of homogeneous semiconductor nano-cylinders, perpendicularly aligned with respect to a substrate, and immersed in air. We assume cylinders having diameters in the subwavelength range (order of tens of nm) and length comparable or larger with respect to the wavelength. This structure is characterized by a strong optical anisotropy in the transverse plane perpendicular to the cylinder longitudinal axis (i.e. the growth axis), due to the high aspect ratio and permittivity of the individual components. This geometry is inspired to the typical arrangement of epitaxially grown III-V semiconductor nanowires, which have been reported as promising platforms for reflectance manipulation [14-16,18,19]. The optical properties of these systems are affected, among other parameters, by the dimensions of each component and by the average density of the nanostructures. In our specific case, in order to better study the involved phenomena, we considered, as a starting point, a configuration with a relatively low density of NWs and quite low covering of the growth substrate with NWs (about 10 NWs per micron squared, with an inter-distance among every element of about a few hundreds of nm). In these conditions, the far field reflectance of the system has a flat curve, very similar to that of the bare substrate [27], thus not very interesting from an optical point of view. Starting from this platform, we explore the possibility to induce a non-trivial optical response, by introducing some geometrical modifications in the individual building blocks. The first approach consists in adding a thin shell of a different material around each cylinder, thus realizing a core-shell heterostructured nanowire. The introduction of a shell enhances the system anisotropy in the planar directions parallel to the substrate, by implementing a stepped refractive index contrast. Experimental studies have demonstrated that the presence of a thin shell, even just a ten or a few tens of nanometers, made of a different material with respect to the core, around each individual nanowire, generates an enhancement of the interference phenomena, yielding to marked oscillations in the measured reflectance spectra [27,28]. A further step forward in the modulation of the optical properties of this kind of systems can be obtained by introducing an additional anisotropy along the cylinder longitudinal axis resorting to an inverse - i.e. from the base to the tip - tapered nanostructure shaping. Tapering, i.e. the variation of the cylinder diameter along its longitudinal axis, allows to obtain a further modulation of the refractive index in the direction perpendicular to the substrate due to the inhomogeneity of the refractive index function [29].

Resorting to simulation methods we computationally studied the effect of the specific morphological modifications explained above on the specular reflectance from individual NWs as well as from a random assembly of NWs. We compared the insights offered by our simulations to a set of results previously reported for random assemblies of III-V semiconductor nanowires [27]. State of the art self-assembling growth techniques, such as the chemical beam epitaxy, in fact, enable the growth of very pure crystal phase semiconductor materials as well as extremely fine controlled axial and radial heterostructures, without any additional fabrication step after growth [30-37]. Following Ref. [27], we considered three samples i.e. a random array of homogeneous GaAs NWs, an assembly of GaAs/AlGaAs core-shell (CS) NWs with fixed diameter along the NW axis and an assembly of tapered GaAs/AlGaAs CS NWs (the tip of the nanowires having a larger diameter with respect to the base). Taking into account our theoretical results, we discuss the dependence of the reflection properties on the individual NW structure and the angle-resolved specular reflectance for the three assemblies of NWs.

SAMPLE MODELS AND SIMULATIONS

Sample Models

We considered three models of NW samples, labeled as Model A, B and C. Model A consists of a random ensemble of homogeneous semiconductor nano-cylinders, having diameter d = 55 nm and average length L = 860 nm. Model B consists of a random ensemble of not-tapered CS NWs with core diameter d_{CORE} = 55 nm, shell thickness of 30 = nm (for a total NW diameter d_{NW} = 115nm), and length L = 1300 nm. Model C consists of a random ensemble of tapered CS NWs with core diameter d_{CORE} = 55 nm, shell thickness ranging from 30 nm (at the base) and 55 nm (at the tip) (for a total NW diameter at the base d_{BASE} = 115 nm and a total NW diameter at the tip d_{TIP} = 165 nm) and length L = 1400 nm. The core structure is the same for all the three models. In Model B we added to each cylinder a 30 nm thick shell. Model C is identical to model B at the base, but we introduced a modulation in the shell thickness, in order to have a shell thickness at the tip as large as the core diameter. Small deviations in the shape and dimensions of the NWs, with respect the theoretical values used in our models, were reported for the real samples investigated in Ref. [27] and considered as test-bed of the design approach proposed in the present work. In particular, we simplify the systems under study assuming a cylindrical symmetry of the NWs rather than a

hexagonal one. However, within the admitted growth tolerances identified during the simulation procedure, we just adapted the model parameters to the experimental values (determined by scanning electron microscopy) in order to match at the best of our capabilities the theoretical and the experimental results.

Analytical Simulations

In order to study the reflectance behavior in the far field, we modelled our system by using an effective medium approximation. This approach was reported to well describe the optical behavior of vertical assemblies of subwavelength cylindrical nanostructures in a relatively broad spectral range [16, 38-40]. The effective medium model aims at approximating complex electromagnetic media, with a homogeneous effective medium, by averaging the multiple specific parameters of each of its components. The medium dielectric constant can be expressed in terms of the dielectric constants and volume fraction of the individual components. In order to analytically calculate the specular reflectance (R) for ideal samples corresponding to the models labelled as A and B and schematically depicted in Fig. 1a-b, we assumed a medium composed of GaAs core cylinders with dielectric constant $\varepsilon_{\mathrm{GaAs}}$ (Model A), possibly surrounded by a shell of AlGaAs with dielectric constant $\varepsilon_{\mathrm{AlGaAs}}$ (Model B), with a substrate filling factor (fraction of the substrate area covered by NWs) p with $0 \leq p \leq 1$, immersed in air (background). In particular, for the calculations we used the dielectric constant of $Al_xGa_{1-x}As$ for x = 0.1. For the case of Model C i.e. tapered NWs (see Fig. 1c), analytical calculations are performed by considering an ensemble of vertical NWs with core diameter d_{CORE}=55 nm and an average shell thickness of 42.5 nm. As the formulas are quite general, in the model description, we will indicate with a subscript "C" the parameters related to the cylinder material, and with a subscript "B" the parameters related to the background material in which the cylinders are immersed. The effective dielectric constant over the transverse plane perpendicular to the cylinder axis, $\varepsilon_{\perp}$, can be expressed by using the Maxwell-Garnett mixing formula:

$$\varepsilon_{\perp} = \left[pf_C\varepsilon_C + (1-p)\varepsilon_B \right] \Big/ \left[pf_C + (1-p) \right] \tag{1}$$

where $f_C = 2\varepsilon_B/(\varepsilon_C + \varepsilon_B)$, $\eta = \left(d_{\mathrm{NW}}/d_{\mathrm{CORE}}\right)^2$, d_{NW} and d_{CORE} represent the NW external diameter and the NW core, respectively, and

$$\varepsilon_C = \varepsilon_{\mathrm{AlGaAs}} \left[\left(\varepsilon_{\mathrm{GaAs}} + \varepsilon_{\mathrm{AlGaAs}}\right) + \eta\left(\varepsilon_{\mathrm{GaAs}} - \varepsilon_{\mathrm{AlGaAs}}\right) \right] \Big/ \left[\left(\varepsilon_{\mathrm{GaAs}} + \varepsilon_{\mathrm{AlGaAs}}\right) - \eta\left(\varepsilon_{\mathrm{GaAs}} - \varepsilon_{\mathrm{AlGaAs}}\right) \right] \tag{2}$$

The effective dielectric constant over the cylinder axis can be express as an arithmetic average:

$$\varepsilon_z = p\varepsilon_C + (1-p)\varepsilon_B \tag{3}$$

Following previous studies [40] that suggest that the gold catalyzer on top of the NWs has not a noticeable influence on the optical response, we neglected the contribution of this component. Then we calculated the optical propagation of monochromatic waves with angular frequency ω and wavevector $k = (k_x, k_z)$ impinging on the effective-medium described above. Two analytical sub-sets of solutions for transverse electric (TE-) and transverse magnetic (TM-) polarized waves were obtained as solution of the Maxwell's equations.

Numerical Simulations

A second simulation approach was also used, based on the full solution of the Maxwell equations in space and time domain in complex media by means of FDTD numerical methods. In particular, we performed FDTD simulations of the electric field spatial distribution and of the specular reflectance, using the commercially available software Lumerical® FDTD Solutions [41].This method has the advantage to address the far- and near-field response without any assumption of approximation. For the calculations, three system models were designed, composed by as a quasi-random array of vertically-aligned identical NWs [42]. The electric field distribution and reflectance spectra were calculated for several horizontal planes at different distances along the z axis from the upper surface of the substrate.

RESULTS AND DISCUSSION

In Fig. 1 we show a graphical representation of the three steps behind the proposed approaches for enhancing the modulation of the reflectance spectra. In particular, Fig. 1a, b and c show schematics of the three models associated with each steps. We consider NW heterostructures made of two generic semiconductors, labeled 1 and 2. Model A (Fig. 1a) represents the basic considered configuration i.e. a random ensemble of homogeneous nano-cylinders, perpendicularly aligned with respect to a substrate. Concerning Model B (Fig. 1b), we try to introduce a modulation in the optical reflectance by adding a thin shell of a different material around each cylinder, thus realizing an assembly of core-shell NW heterostructures. In Model C (Fig. 1c), we introduce anisotropy (tapering) along the cylinder axis by assuming a shell with a variable thickness. Figure 1d, e and f reports a sketch of the expected reflectance behavior for Model A, B and C, respectively, assuming to measure the specular reflectance at a fixed angle and varying the wavelength λ of the incident light.

For Model A, when the filling factor of the cylinder is quite low, we don't expect any strong feature in the optical reflectance spectrum [43,44], but we rather expect an almost flat behavior similar to the one of the bare substrate (Fig. 1d). The addition of a shell, in Model B, likely enhances the system anisotropy in the planar directions parallel to the substrate, resulting in the appearance of modulations in the reflectance spectrum (Fig. 1e). Finally, the introduction of tapering, in Model C, is expected to induce very marked oscillations in the reflectance spectra (Fig. 1f).

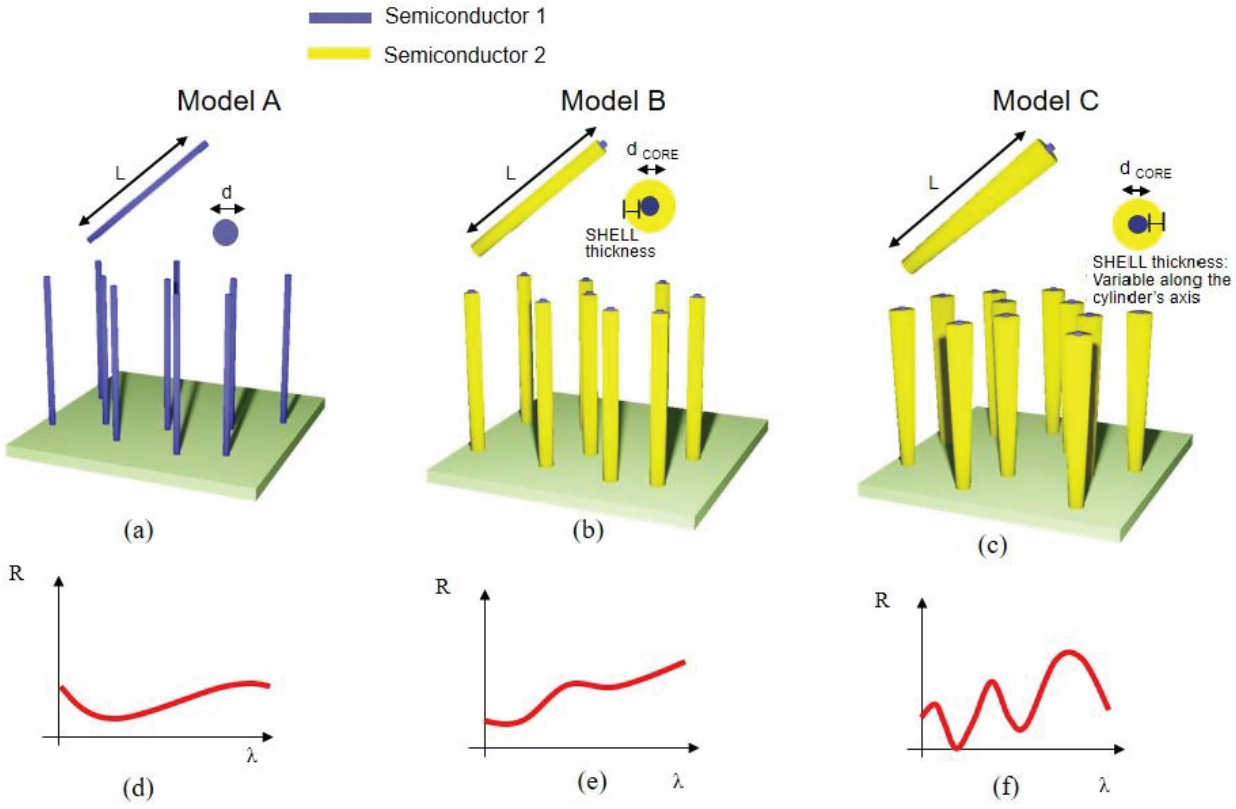

FIGURE 1. (a-c) Schematic representation of the geometrical features of the three nanowire sample models investigated in this work: (a) Model A: not-tapered homogeneous cylinder array; (b) Model B: not-tapered core-shell cylinder array; (c) Model C: tapered core-shell cylinder array. (d-f) Expected reflectance (R) behavior *versus* wavelength λ for the three models schematically reported in panels (a-c).

Within the frame of our analytical simulations, we calculated the full analytical solutions of Maxwell's equations within the homogeneous medium approximation by considering two sub-sets of solutions for TE- and TM-polarized waves, and solving them by the transfer matrix approach for the considered configurations labeled Model A, Model

B and Model C. Regarding the semiconductor materials labeled as "Semiconductor 1" (or "core") and "Semiconductor 2" (or "shell") in Fig. 1, we select GaAs and AlGaAs, respectively.

The results are reported in Fig. 2 which displays the color plot of the reflectance (R) as a function of the light incident angle, θ, and the excitation wavelength, λ, analytically calculated for the Models A, B and C and for the two polarizations TE- and TM-. Panels (a) and (b) of Fig. 2 report for the homogeneous cylinder configuration corresponding to Model A, the calculated reflectance for TE- and TM-polarized waves, respectively. The two datasets are almost featureless, in particular as function of the wavelength, consistently with the relatively low density of the NWs and the very low covering of the growth substrate with NWs: the sample overall behaves quite similarly to a bare substrate. On the contrary, for the CS NWs (Model B) and tapered core-shell (Model C) samples, the behavior of the specular reflectance as a function of the incident wavelength and angle display marked modulations, as can be evinced from Fig. 2c,d (Model B) and Fig. 2e,f (Model C). These features are significantly enhanced when incident light has TE-polarization (Fig. 2c,e), with the occurrence of clear oscillations of the reflectance. This can be tentatively ascribed to the small scattering cross-section of the outer shell for a TM-polarized light beam [23]. In addition, we observe that as the incidence angle θ increases, the reflectance peaks overall shift towards lower wavelengths, for both Model B and Model C. Noticeably, the differences between panel (c) and panel (e) are almost negligible, i.e., the tapering of the core-shell NWs does not really affect the amplitude of the reflectance oscillations: this is a direct consequence of the effective medium approximation, which does not effectively take into account the specific geometrical features of the individual scatters, but rather considers a homogeneous effective medium with averaged optical properties.

On the one hand, the analytical model allows to identify the occurrence of reflectance modulations and the rough dependence on the incidence angle θ and wavelength λ, and, as will be pointed in the discussion of last figure of this Section, the model reproduces qualitatively the main experimental trends. On the other hand, effective medium model does not precisely take into account neither the role of the multiple reflectance occurring at the different interfaces air-shell and core-shell, nor the effect of tapering.

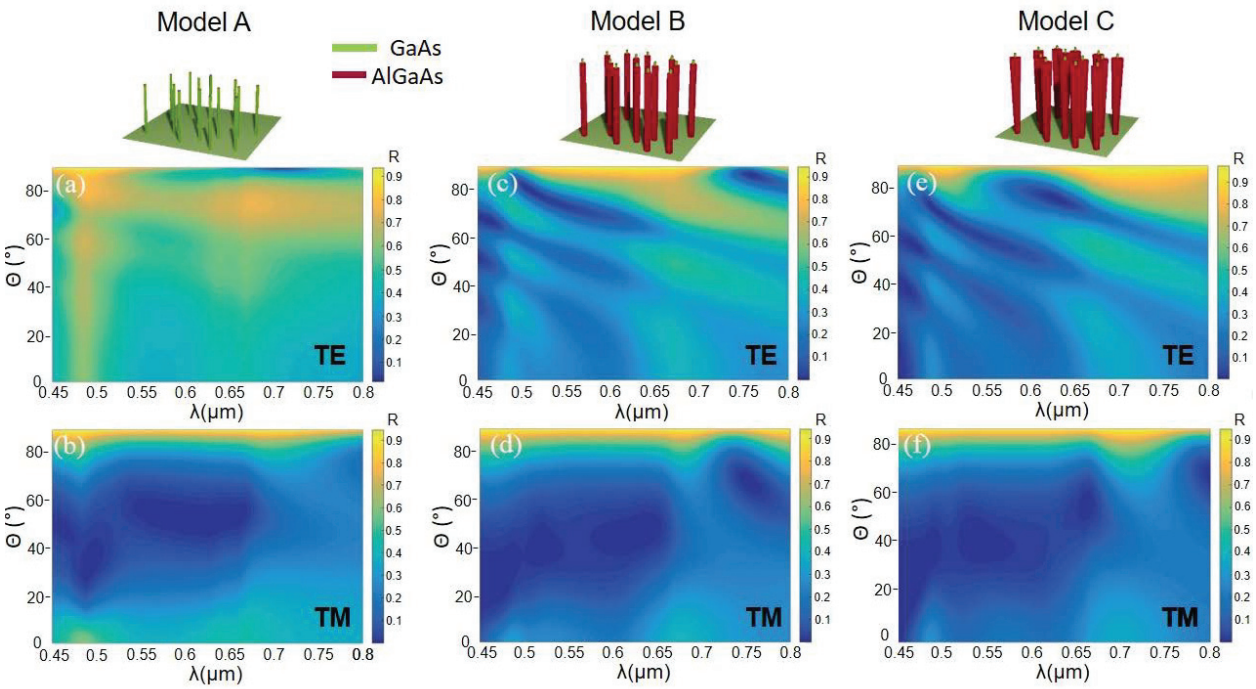

FIGURE 2. Specular reflectance analytically calculated within the effective medium model as a function of the incident angle θ (in the range from 0 to 90 deg) and wavelength λ (in the range from 0.45 to 0.8 μm) for the three NW sample models, i.e. Model A (homogeneous GaAs NWs), Model B (not tapered CS GaAs/AlGaAs NWs) and Model C (tapered CS GaAs/AlGaAs NWs). Panels (a), (c) and (e) correspond to incident light with TE-polarization, while panels (b), (d) and (f) correspond to incident light with TM-polarization.

Regarding the numerical approach, first of all we performed FDTD numerical simulations to investigate the spatial distribution of the TE-polarized electric field in proximity of each individual NW as a function of the incident angle. In order to perform the simulations we refer to the semiconductor materials and the geometrical features of three NW samples investigated in Ref. [27], that qualitatively correspond to the three NW sample Models (labeled "A", "B" and "C") presented and discussed in the previous sections. In Fig. 3, the left panels (not labeled) display a pictorial representation of an individual NW for each of the three considered samples, providing full information on the semiconductor materials (wurtzite GaAs for the "core" and AlGaAs for the "shell") and the geometrical parameters i.e. the shape (hexagonal cross-section), the average diameter, d_{NW}, and the average length, L. In the presence of NW tapering, the diameter at the base of the NW ($d_{NW\ BASE}$) differs from the one at the tip of the NW ($d_{NW\ TIP}$). We assumed the same numerical values reported in Ref. [27]. Based on the results of our previous works, in particular Ref. [20], and on preliminary simulations, for the full calculations of the specular reflectance we simplify the systems under study assuming a cylindrical symmetry of the NWs rather than a hexagonal one. We evaluated the electric field expansion intensity along the axial sections lengths of the cylindrical NWs and the electric field expansion intensity distribution along transverse planes perpendicular to the NW axis, and in Fig. 3 we report the results of the FDTD numerical simulation.

The spatial distribution of the near field normalized longitudinal electric field intensity ($E/E_{inc.}$) around an individual NW is reported in panel (a), (c) and (e) respectively for a homogeneous GaAs nanowire, a not-tapered CS GaAs/AlGaAs NW and a tapered CS GaAs/AlGaAs NW, at incident angles $\theta = 0°$ and $\theta = 70°$. The X-Y plane correspond to the substrate, while the Z coordinate corresponds to the growth axis and defines the NW length. Panels (b), (d) and (e) report the near-field normalized transversal electric field intensity ($E/E_{inc.}$) distribution on the XY-plane for Z = 200 nm at an incident angle $\theta = 70°$ for a random array of homogeneous GaAs NW (Fig. 3b), not-tapered CS GaAs/AlGaAs NWs (Fig. 3d) and tapered CS GaAs/AlGaAs NWs (Fig. 3f). The exact locations of the NWs are indicated with asterisks. The results of the FDTD simulations for the electric field distributions, in both the longitudinal and transverse directions, show that by controlling the geometry of the individual scatterer (the NW) it is possible to modify the electric field distribution on a relatively wide area. The increase in the incident angle (e.g. from $\theta = 0°$ to $\theta = 90°$) corresponds to a shift of the maximum of the electric field distribution from the upper part of the NW towards the NW bottom, promoting the coupling between each individual nanostructure and the substrate. However, Fig. 3b and 3d show that for not tapered NWs the electric field remains confined in proximity of the individual NW (even at high incident angle), without any substantial intra-NW or substrate-NW interaction. Instead, Fig. 3f shows that a substantial difference occur for tapered NWs: we observe in fact a strong reduction of the confinement of the electromagnetic field around the single NW, with a remarkable spreading in the free space between different NWs. These results indicate that the tapered NW morphology enhances the reciprocal coupling between different NWs, and the coupling of individual NWs with the substrate.

In Fig. 4 we report a selection of theoretical as well as experimental reflectance spectra, in order to compare the results of the analytical and numerical simulations and to discuss their ability to reproduce the experimental trends observed in real samples. All spectra reported in Fig. 4 correspond to TE-polarized incident light covering the visible and near-IR range, and three different incident angles ($\theta = 10°$, 40° and 70°). In Fig. 4, the left panels (not labeled) display a pictorial representation of the three considered NW samples, namely GaAs NWs as well as untapered and tapered CS GaAs/AlGaAs NWs.

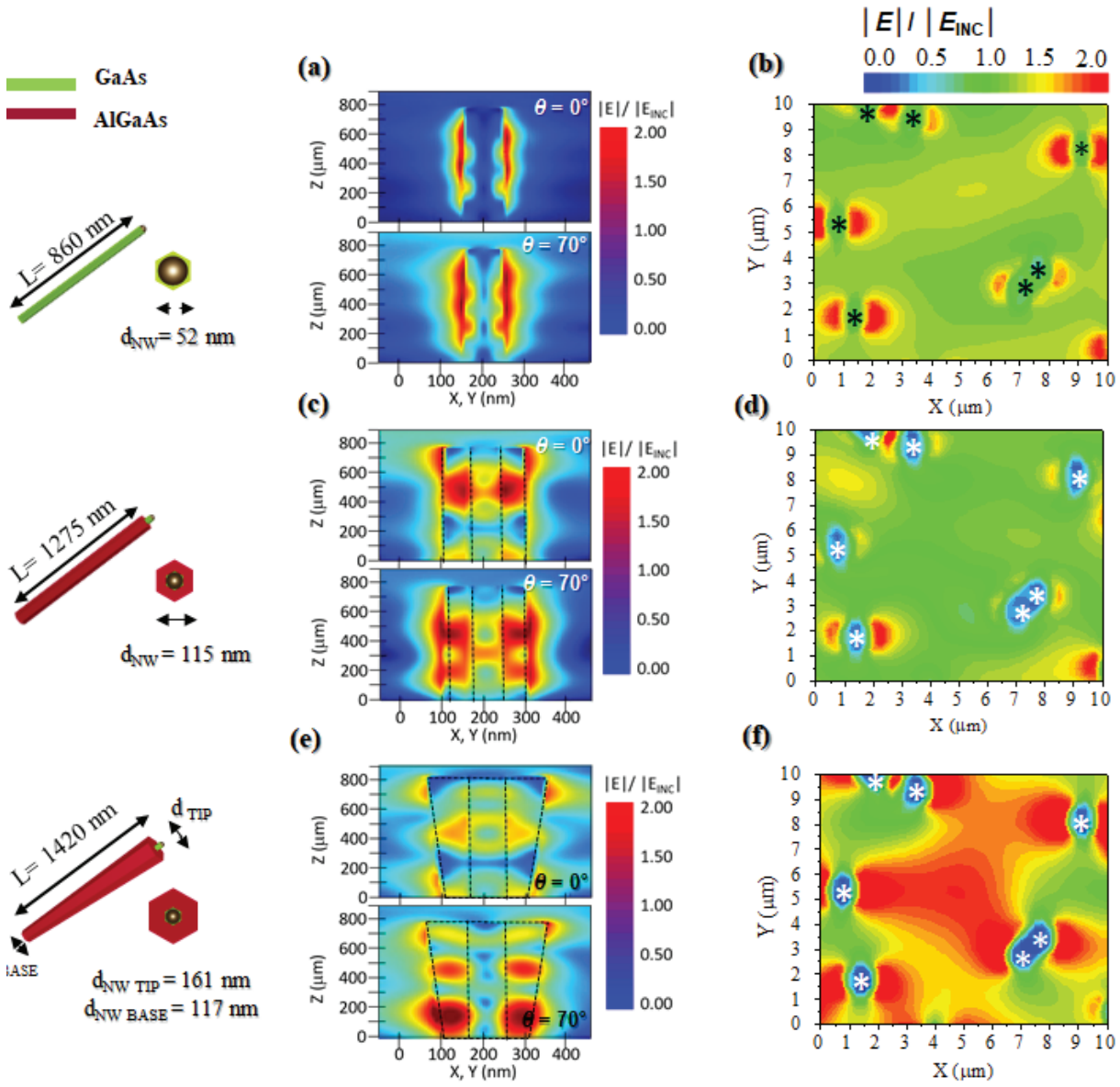

FIGURE 3. Normalized TE-polarized electric field distribution intensity around a single cylinder at incident angles $\theta = 0°$ and $\theta = 70°$ for (a) homogeneous GaAs NW at $\lambda = 850$ nm, (c) untapered CS GaAs/AlGaAs NW at $\lambda = 735$ nm, (e) tapered CS GaAs/AlGaAs NW at $\lambda = 925$ nm. Near-field normalized transversal electric field intensity distribution in the XY-plane at Z = 200nm and $\theta = 70°$ for (b) homogeneous GaAs NW at $\lambda = 850$ nm, (d) untapered CS GaAs/AlGaAs NW at $\lambda = 735$ nm and (f) tapered CS GaAs/AlGaAs NW at $\lambda = 925$ nm.

Figure 4a, 4d and 4g show the reflectance of a random assembly of homogeneous GaAs NWs with relatively low NWs density (10 NW μm^{-2}) and low covering of the growth substrate, calculated analytically (panel a), simulated numerically (panel d) and measured experimentally as reported in Ref. [27] (panel g). The experimental data reported in panel (g) reveal almost featureless reflectance spectra, with a weak peak barely observable at about 850 nm, likely due to the bulk GaAs substrate. FDTD simulations reported in panel (d) accurately reproduces the reflectance features, while the results of the effective medium method reported in panel (a) are less accurate, and only reproduce very qualitatively the reflectance trends.

Figure 4b, 4e and 4h show the reflectance of a random assembly of untapered core-shell GaAs/AlGaAs NWs calculated analytically (panel b), simulated numerically (panel e) and measured experimentally as reported in Ref. [27] (panel h). For incident angles $\theta = 10°$ and 40°, in the experimental as well as numerically simulated spectra

reported in panels (h) and (e), respectively, the mean reflectance amplitude is lower with respect to the case of homogenous GaAs NW sample, with an almost negligible signal for wavelengths lower than about 550 nm. At high incident angles (θ = 70°), the onset of modulations of the reflectance starts to be visible. These incipient reflectance modulations may evolve into oscillations and are likely due to interference effects arising from the presence of a double scattering interface (air-shell interface and core-shell one), that gives rise to a refractive index grading. This behavior is somehow over-emphasized from the analytical simulations, that return over-estimated reflectance oscillation amplitude, as evident in panel (b).

Figure 4c, 4f and 4i show the reflectance of a random assembly of tapered CS GaAs/AlGaAs NWs calculated analytically (panel c), simulated numerically (panel f) and measured experimentally as reported in Ref. [27] (panel i). The strong increase of the sample anisotropy due to the tapering of the NWs, corresponding to an increasing thickness of the AlGaAs shell from the bottom to the tip of the NW, returns extremely marked oscillations in the specular reflectance, as can be seen very clearly in the experimental as well as numerically simulated spectra reported in panels (i) and (f), respectively. These oscillations occur for every incident angles and the reflectance has a non-vanishing value in all the explored spectral range. The position (wavelength) and intensity of each reflectance peak vary with the incident angle. The results obtained from the analytical model are reported in panel (c) and show that, despite the occurrence of marked reflectance oscillations, the model is poorly accurate in reproducing the strong enhancement of the oscillating behavior due to the tapered geometry, as well as the evolution of peaks and dips as function of λ and θ. FDTD simulations allow instead to better reproduce the experimental spectra, highlighting the role of the morphological properties of the individual NWs to determine the global optical response of the NW assembly.

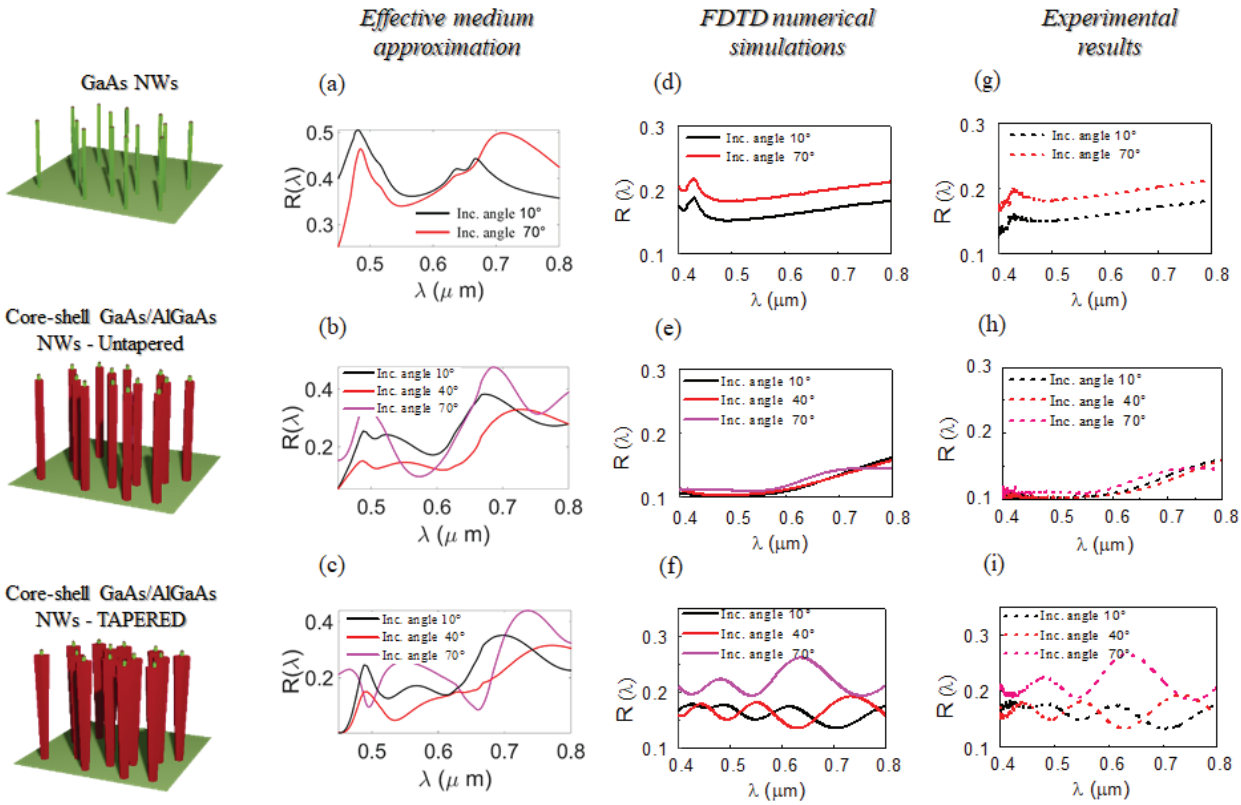

FIGURE 4. Theoretical and experimental reflectance spectra from random assemblies of homogeneous GaAs NWs (a, d, g), untapered CS GaAs/AlGaAs NWs (b, e, h), and tapered CS GaAs/AlGaAs NWs, for TE-polarized incident light from visible to near-IR energy range, and incident angle θ = 10°, 40°, 70°. Results from analytical simulations are reported in panels (a-c). Results from numerical FDTD simulations are reported in panels (d-f). Experimental results from Ref. [27] are reported in panels (g-i).

CONCLUSIONS

In conclusion, we report a strategy to control and enhance the modulation of the optical response of random assembly of vertically aligned subwavelength semiconductor nanostructures. By resorting to analytical and numerical simulations, we show that marked broadband intensity modulations of the specular reflectance of a randomly arranged NW assembly can be obtained by exploiting a core-shell morphology and by tapering the individual NWs to induce a strong refractive index anisotropy. Analytical simulations can be useful to grasp the far field optical response, neglecting the detailed morphology of the NWs and assuming a homogeneous medium with optical properties calculated as a mixing of those of its components. The FDTD numerical approach allows, instead, to evaluate both the near field properties and the far field response, allowing to investigate the reflectance phenomena occurring at the nanoscale of the individual NW together with the global reflectance response of the NW assembly. For sake of completeness, the results of our analytical as well as numerical simulations were comparatively discussed and compared to experimental results previously reported for random assemblies of GaAs NWs as well as untapered and tapered CS GaAs/AlGaAs NWs. Our approach is especially promising in the context of the epitaxial growth of semiconductor nanowires, where complex morphologies and heterostructures can be engineered directly exploiting the bottom-up growth of the nanostructures.

ACKNOWLEDGMENTS

We acknowledge the financial support by the program PRIN 2017 for the Project "Photonic Extreme Learning Machine" (PELM), protocol number 20177PSCKT.

REFERENCES

1. N. Yu, F. Capasso, Nat. Mater. **13**, 139-150 (2014).
2. N. Yu, P. Genevet, MA. Kats, F. Aieta, JP.Tetienne, F. Capasso, Z. Gaburro, Science **334**, 337-337 (2011).
3. A.V. Kildishev, A. Boltasseva, V.M. Shalaev. Science **339**, 1232009 (2013).
4. S. Wuestnerand,O. Hess, Progress in Optics **59**, 1-88 (2014).
5. M. Kauranen, A.V. Zayats, Nat. Photonics **6**, 737-748 (2012).
6. F. Lemoult, N. Kaina, M. Fink, G. Lerosey, Nat. Phys. **9**, 55-60 (2013).
7. D. Neshev, I. Aharonovich, Light: Science & Applications **7**, 58 (2018).
8. S. M. Kamali, E. Arbabi, A. Arbabi , A. Faraon, Nanophotonics **7**, 1041–1068 (2018).
9. A.C. Overvig, S. Shrestha, S.C. Malek, M. Lu, A. Stein, C. Zheng, N. Yu, Light Sci. Appl. **8**, 92 (2019).
10. P. B. Johnson, R. W. Christy, Phys. Rev. B **6**, 4370–4379 (1972).
11. J. B. Khurgin,.G. Sun, Appl. Phys. Lett. **100**, 011105 (2012).
12. B. Slovick, Z. Yu, M. Berding, S. Krishnamurthy, Phys. Rev. B **88**, 165116(2013).
13. F. Aieta, M.A. Kats, P. Genevet, F. Capasso, Science **347**, 1342 (2015).
14. I. Staude, J. Schilling, Nat. Photonics **11**, 274 (2017).
15. N. Künzner, D. Kovalev, J. Diener, E. Gross, V.Y. Timoshenko, G. Polisski, M. Fujii, Optics Letters **26**, 1265 (2001).
16. W. A. De Heer, W. S. Bacsa, A. Chatelain, T. Gerfin, R. Humphrey- Baker, L. Forro, D. Ugarte, Science **268**, 845 (1995).
17. Z.P. Yang, L. Ci, J.A. Bur, S.Y. Lin, P.M. Ajayan, Nano Lett. **8**, 446– 451 (2008).
18. O.L. Muskens, S.L.Diedenhofen, M.H.M. Van Weert, M.T. Borgström, E.P Bakkers, E.P.A.M.; J. Gómez-Rivas, Adv. Funct. Mater. **18**, 1039–1046 (2008).
19. O.L.,Muskens, M.T. Borgström, E.P.A.M. Bakkers, J. Gómez-Rivas, J. Appl. Phys. Lett. **89**, 233117 (2006).
20. F. Floris, L. Fornasari, A. Marini, V. Bellani, F. Banfi ,S. Roddaro, D. Ercolani, M. Rocci , F. Beltram, M. Cecchini, L. Sorba, F. Rossella, Nanomaterials **7**, 400 (2017).
21. E. Gross, D. Kovalev, N. Künzner, V. Yu. Timoshenko, J. Diener, and F. Koch, Journal of Applied Physics **90**, 3529 (2001).
22. M. L. Brongersma, Y. Cui, S. Fan, Nat. Mater. **13**, 451–460 (2014).
23. E. Garnett, P.Yang, Nano Lett. **10**, 1082–1087 (2010).

24. O. L. Muskens, J. Gómez Rivas, R. E. Algra, E.P. A. M. Bakkers, A. Lagendijk., Nano Lett. **8**, 2638–2642 (2008).
25. Y. Zhao, A. Alù, Phys. Rev. B **84**, 205428 (2011).
26. B. Wang, F. Dong, Q.T. Li, D.Yang, C. Sun, J. Chen, Z. Song, L. Xu, W. Chu, Y.F. Xiao, Q. Gong, L. Yan, Nano Lett. **16**, 5235–5240 (2016).
27. F. Floris, L. Fornasari, V. Bellani, A. Marini, F. Banfi, F. Marabelli, F. Beltram, D. Ercolani, S. Battiato, L. Sorba, F. Rossella, Materials **12**, 3572 (2019).
28. S L. Diedenhofen, J. Gómez Rivas, Semicond. Sci. Technol. **25**, 024008 (2010)..
29. Y. Kurokawa, S. Kato, M. Konagai, Proc. SPIE 9178, Next Generation Technologies for Solar Energy Conversion V, 91780N (2014).
30. V. Demontis, M. Rocci, M. Donarelli, R. Maiti, V. Zannier, F. Beltram, L. Sorba, S. Roddaro, F. Rossella, C. Baratto, Sensors **19**, 2994 (2019).
31. J. Lieb, V. Demontis, D. Prete, D. Ercolani, V. Zannier, L. Sorba, S. Ono, F. Beltram, B. Sacepe, F. Rossella, Adv. Funct. Mater. **1804378** (2019).
32. A. Arcangeli, F. Rossella, A. Tomadin, J. Xu, D. Ercolani, L. Sorba, F. Beltram, A. Tredicucci, M. Polini, S. Roddaro, Nano Lett. **16**, 5688–5693 (2016).
33. D. Prete, P. Erdman, V. Demontis, V. Zannier, D. Ercolani, L. Sorba, F. Rossella, F. Taddei, S. Roddaro, Nano Lett. **19**, 3033−3039 (2019).
34. M. Rocci, F. Rossella, U.P. Gomes, V. Zannier, F. Rossi, D. Ercolani, L. Sorba, F. Beltram, S. Roddaro, Nano Lett. **16**, 7950-7955 (2016).
35. S. Salimian, O. Arif, V. Zannier, D. Ercolani, F. Rossi, Z.S. Momtaz, F. Beltram, S. Roddaro, F. Rossella, L. Sorba, Nano Research, **13**, 1065–1070 (2020).
36. S. Battiato, S. Wu, V. Zannier, A. Bertoni, G. Goldoni, A. Li, S. Xiao, X.D. Han, F. Beltram, L. Sorba, X.Xu, F. Rossella, Nanotechnology **30,** 194004 (2019).
37. S. Wu, K. Peng, S. Battiato, V. Zannier, A. Bertoni, G. Goldoni, X. Xie, J. Yang, S. Xiao, C. Qian, F. Song, S. Sun, J. Dang, Y. Yu, F. Beltram, L. Sorba, A. Li, B.-b. Li, F. Rossella, X. Xu, Nano Research **12**, 2842–2848 (2019).
38. J. C. M. Garnett, Philos. Trans. R. Soc. London A **203**, 385–420 (1904).
39. R.J. Pollard, A. Murphy, W.R. Hendren, P.R. Evans, R: Atkinson, G.A. Wurtz, A.V. Zayats, V.A: Podolskiy, Phys. Rev. Lett. **102**, 127405 (2009).
40. J. Elser, R. Wangberg, V. A. Podolskiy, E.E. Narimanov, Appl. Phys. Lett. **89**, 261102 (2006).
41. Lumerical Inc. Available online: http://www.lumerical.com/tcad-products/fdtd/ (accessed on 1 March 2019).
42. F. Floris, C. Figus, L. Fornasari, M. Patrini, P. Pellacani, G. Marchesini, A. Valsesia, F. Artizzu,, D. Marongiu, M. Saba, A. Mura, G. Bongiovanni, F. Marabelli, F. Quochi, J. Phys. Chem. Lett. **5**, 2935−2940 (2014).
43. Soldano, F. Rossella, V. Bellani, S. Giudicatti, S. Kar, ACS Nano **4**, 6573–6578 (2010).
44. J.M. Caridad, D.Mc Closkey, F. Rossella, V. Bellani, J. F. Donegan, V. Krstić, ACS Photonics **2**, 675-679 (2015).